tvst

Article

Subretinal Saline Protects the Neuroretina From Thermic Damage During Laser Induction of Experimental Choroidal Neovascularization in Pigs

Silja Hansen[1,2], Anne Louise Askou[1], Morten la Cour[3], Thomas J. Corydon[1,2], and Toke Bek[2]

[1] Department of Biomedicine, Aarhus University, Aarhus, Denmark
[2] Department of Ophthalmology, Aarhus University Hospital, Aarhus, Denmark
[3] Department of Ophthalmology, Rigshospitalet, Copenhagen, Denmark

Correspondence: Silja Hansen, Department of Biomedicine, Høegh-Guldbergs Gade 10, DK-Aarhus C, Denmark.
e-mail: silja.hansen@biomed.au.dk

Received: March 24, 2021
Accepted: May 17, 2021
Published: June 29, 2021

Keywords: porcine model; experimental choroidal neovascularization; fluorescein angiography

Citation: Hansen S, Askou AL, la Cour M, Corydon TJ, Bek T. Subretinal saline protects the neuroretina from thermic damage during laser induction of experimental choroidal neovascularization in pigs. Transl Vis Sci Technol. 2021;10(7):29, https://doi.org/10.1167/tvst.10.7.29

Purpose: The purpose of this study was to develop a porcine model for photocoagulation induced choroidal neovascularization (CNV) with high success rate and minimal thermic damage to the neuroretina.

Methods: Experimental CNV was induced by laser photocoagulation in both eyes of 16 domestic pigs. In the left eyes, photocoagulation was preceded by subretinal injection of saline to protect the neuroretina from thermic damage, whereas the right eyes were treated with photocoagulation only. The development of the CNV after 3, 7, 14, 28, and 42 days was evaluated by optical coherence tomography (OCT) scanning, fluorescein angiography, and OCT angiography, and by histology after enucleation.

Results: From day 7 after the photocoagulation, OCT showed subretinal density in all lesions of 14 alive animals, and either fluorescein or OCT angiography confirmed CNV formation in 11 of 14 of the eyes that had received photocoagulation alone and those in which photocoagulation had been preceded by subretinal injection of saline. In all cases pretreated with subretinal saline, the neuroretina was protected from immediate thermic damage. The formation of CNVs were confirmed by histology. For both groups, the largest lesions were observed within 14 days after photocoagulation.

Conclusions: Injection of subretinal saline can protect the retina from thermic damage induced by retinal photocoagulation without reducing the success rate in producing experimental CNV. The effect of interventional studies aimed at reducing photocoagulation induced experimental CNV in pigs can be evaluated within 2 weeks after photocoagulation.

Translational Relevance: This model provides a fundament to develop and evaluate novel treatment methods for neovascular retinal diseases.

Introduction

Age-related macular degeneration (AMD) is the leading cause of visual impairment and blindness among elderly persons in the Western world[1–3] and the incidence is expected to increase further.[4] The disease can develop into two sight-threatening forms (i.e. dry or non-neovascular AMD, and wet or neovascular AMD [nAMD]).[5] The latter form is characterized by invasion of new vessels from the choroid (CNV) causing irreversible damage to the retinal tissue.[6] Vascular endothelial growth factor (VEGF) is an important driver for CNV development[7] and the introduction of anti-VEGF antibodies for intravitreal injection has improved the treatment of nAMD significantly.[8] However, the need for frequent injections cumulates the risk for complications and constitutes a significant cost burden for the health care system.[9] Therefore, there is a need for the development of new therapies for nAMD with a more permanent effect. One such approach could be

gene therapy aimed at downregulating the expression of VEGF in the eyes. It has previously been shown that this approach can inhibit the development of experimental CNV induced by laser photocoagulation in mice.[10–12] A translation of this principle for modulating VEGF expression to humans requires an intermediate step where the therapy is reproduced in a model with dimensions more similar to that of the human eye, such as the porcine eye.[13–15] However, in previous porcine models of laser induced CNV, the success rate has been low and procedures involving photocoagulation have caused significant collateral damage to the neuroretina with gliosis.[16,17] This may have been due to variability of the intervention and that individual factors, such as pigmentation, had resulted in variations in the temperature increase and scattering of light energy to the adjacent retina.[18–20]

Therefore, the purpose of the present study was to develop a porcine model for experimental laser photocoagulation induced CNV with a high success rate and a more individual application of the thermic energy to result in minimal damage to the neuroretina.

Materials and Methods

Experimental Animals

Sixteen female domestic pigs (Danish landrace) 3 months of age and weighing approximately 40 kg were used. The protocol was approved by the Danish Animal Experiments Inspectorate (license number: 2018-15-0201-01518) and followed the Association for Research in Vision and Ophthalmology (ARVO) statement for the use of animals in ophthalmic and vision research.

Induction of Choroidal Neovascularization

At day 0 (D0) the animals were pre-anesthetized with intramuscular injection of 50 mg midazolam (Hameln pharmaceuticals Gmbh, Hameln, Germany) and 250 mg S-Ketamine (S-Ketamine; Pfizer, New York, NY, USA). Subsequently, general anesthesia was induced with 50 to 100 mg propofol (Fresenius Kabi, Bad Homburg vor der Höhe, Germany) and endotracheal intubation and artificial ventilation were commenced. The general anesthesia was maintained by intravenous infusion of 2 to 5 mg/kg/h propofol and 15 microgram/kg/h fentanyl (Braun Group, Frederiksberg, Denmark). Both eyes were anesthetized topically using 0.4% oxybuprocaine eyedrops (Minims Oxybuprocaine hydrochloride; Bausch & Lomb, Surrey, UK) and dilated by topical application of 0.5% tropicamide (Mydrialcyl; Alcon, Rødovre, Denmark) and 10% metaoxedrin (Metaoxedrin; Amgros I/S, Copenhagen, Denmark). The eyelids were kept open using an eyelid holder and saline was frequently applied with a syringe to maintain the corneas were lubricated.

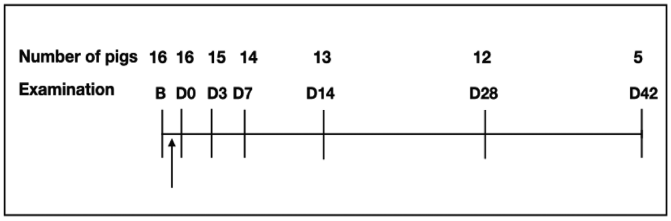

Figure 1. The number of pigs examined at baseline (B) and at the different times of follow-up (D0–D42) after the time of photocoagulation (*arrow*).

The experimental protocol is shown in Figure 1. Baseline (B) images of the retina were obtained with the multimodal retinal imaging device (Deep range imaging (DRI) optical coherence tomography [OCT]-1 Triton plus; Topcon, Roskilde, Denmark), modified by removal of the chin rest to allow examination of porcine eyes in vivo. Radial OCT scans centered on the visual streak were obtained, each with a length of 9.0 mm and an angular separation of 30 degrees. OCT angiography was performed by 6 × 6 mm scans centered on the same area. For visualization of the retina during the following interventions, a surgical microscope (Opmi Lumera 300;, Zeiss, Jena, Germany) combined with a wide angle lens (Biom Ready 200 mm; Oculus Optikgeräte GmbH, Wetzlar, Germany) and a light source (Xenon Bright Star; DORC, Zuidland, The Netherlands) was used.

Focal photocoagulation for the induction of experimental CNV was performed in the horizontally oriented central visual streak in the retina of the right eyes using an IRIS medical Oculight SLx 810 nm laser (810 nm, spot size 600 µm, 800 mW-1 W, for 1 second; Iridex, Mountain View, CA, USA). The laser energy was focused on Bruch's membrane and 3 applications were delivered, separated by at least 800 µm with an effect between 800 mW and 1000 mW. The application that most optimally generated a white spot with a central bubble assumed to be sufficient to induce a neovascular response[21] was chosen as the test application. In the left eyes, two incisions were made nasally and temporally at a distance of 1.2 mm from the corneal limbus. A light probe (Endoillumination Probe; DORC) was introduced through the nasal incision using a vitreo-retinal port system (23 gauge; DORC). The sleeve of a peripheral venous catheter (Venflon, 22G; Becton, Dickinson and Company, Franklin Lakes, NJ, USA) was shortened by 4 mm using a surgical knife (disposable

scalpel; Swann-Morton, Sheffield, England) and was introduced into the vitreous body through the temporal incision until the tip was 1 mm in front of the visual streak. A subretinal cannula (Poly Tip Cannula 23/28 g; MedOne, Sarasota, FL, USA) was advanced through the sleeve to penetrate the neuroretina and 0.05 mL saline was injected to produce a subretinal bleb. Subsequently, a laser application with the same power as that producing the optimal power in the right eye was applied to Bruch's membrane underlying the detached neuroretina. The pars plana incisions were sutured (Ethicon Coated Vicryl 6-0, nr. W9756; Ethicon, Somerville, NJ, USA) and tobramycin 3 mg/mL eyedrops (Tobrex; Alcon) and Viscotears Eye Gel (2 mg/g; Alcon) were applied to the eyes. The anesthesia was maintained for 30 minutes, followed by an examination (D0) that consisted of fundus photography, OCT scanning, and OCT angiography similar to the procedures followed before the photocoagulation. In 6 of the 16 animals, the subretinal injection of saline was accompanied with a minor hemorrhage at the site of the retinotomy, which had been resolved at the following examination. Two animals in which the subretinal injection caused a severe vitreous hemorrhage were replaced. No cases of retinal detachment were observed. After recovery from anesthesia, the animals were kept in a stable in groups of two. In order to limit irritation of the eyes, the stable light was dimmed during the first 2 days after the intervention. Furthermore, regular inspection of the animals was performed by a veterinarian nurse.

Evaluation of CNV Formation

In vivo follow-up examinations were performed on days 3, 7, 14, 28, and 42 (D3–D42) after the photocoagulation (see Fig. 1). At each examination, the animal was sedated by intramuscular injection of 10 mL mixture containing: Zoletil (125 mg tiletamine and 125 mg zolapam; Virbac, Carros, France), 6.25 mL xylazine (20 mg/mL, Rompun; Bayer, Leverkusen, Germany) 1.25 mL ketamine (100 mg/ml, Ketaminol, MSD Animal Health, Copenhagen, Denmark), and 2.5 mL butorphanol (10 mg/ml, Torbugesic, Zoetis, Parsippany, NJ, USA). Sedation was maintained by intravenous injection of Propofol 10 to 50 mg/h while the animal breathed 100% oxygen delivered through a mask (E-vet A/S, Haderslev, Denmark), which was connected to a respirator (Datex Ohmeda S5 Advanced, GE Healthcare Denmark A/S, Brøndby, Denmark). A scleral suture was positioned in order to rotate the eye to be aligned with the imaging system. Fundus photography, OCT scanning, and OCT angiography were performed similarly to the procedures on the day of the photocoagulation, and was supplemented with fluorescein angiography after intravenous injection of 2.5 mL fluorescein (100 mg/mL; Paranova, Herlev, Denmark) over 30 seconds. Angiograms were taken during the filling phase (within 10 seconds), the distribution phase (after 60 seconds), and in the late phase (after 5 minutes) after fluorescein injection.

At each follow-up time from D3 to D28, one animal was euthanized after the in vivo imaging procedures using intravenous injection of 0.2 mL/kg pentobarbital (400 mg/mL; Exagon, Richter Pharma, Wels, Germany), and both eyes were enucleated for immunohistochemical examination. This left one less animal to be examined at each following examination. At D28, seven animals were euthanized, which resulted in the following number of animals available for the in vivo examinations: (D0: $n = 16$; D3: $n = 15$; D7: $n = 14$; D14: $n = 13$; D28: $n = 12$; and D42: $n = 5$; see Fig. 1).

Ex Vivo Examinations

The enucleated eyes were fixated for 10 minutes in neutral formalin buffer 10% (CellPath Ltd., Newton Powys, UK). A frontal cut was made at the ora serrata, and the anterior part of the eye was removed. The remaining posterior eye cup was fixated in neutral formalin buffer at room temperature overnight. The area containing the laser application was identified under a light microscope (Leica CLS, 10X; Leica, Wetzlar, Germany), and an area extending at least 3 mm on each side of the lesion was separated to a depth including both the retina and the choroid using a surgical knife (disposable scalpel; Swann-Morton, Sheffield, UK). After dehydration and paraffin embedding, 4 µm sections were cut, and every tenth section was stained with hematoxylin and eosin and mounted on glass slides. The sections containing the laser application were identified in light microscope (VS120 Virtual Slide Microscope; Olympus, Tokyo, Japan) and were documented with its inbuilt camera (CellSense Dimension; Olympus). For each section containing a part of the laser application, the following section was selected for immunohistochemistry. After deparaffination in Xylen (Merck, Darmstadt, Germany), each of these sections were placed in citrate-buffer (2.1 g citrate monohydrate/l, pH 6,0) and were heated in a microwave oven at 85°C for 3 × 3 minutes. The sections were placed on a rocking table for 30 minutes in order to adapt to room temperature, and were washed 3 times with phosphate buffered saline (PBS; pH 7,4) and incubated with PBS + 2% BSA for 10 minutes. Subsequently, the sections were incubated with the endothelial cell marker Griffonia

Simplicifolia Lectin I, isolectin B4 (GSL I, isolectin B4; Vector Laboratories, Burlingame, CA, USA; diluted 1:50 in PBS +1% BSA) at 4°C overnight. The following day, the sections were washed 3 times in PBS at room temperature, stained with 4′,6-diamidino-2-phenylindole (DAPI; 2 mg/mL; Sigma, St. Louis, MO, USA), rinsed twice in distilled water, dipped in ethanol, and dried. LifterSlip premium printed cover glasses (Erie Scientific Company, Portsmouth, NH, USA) were applied using ProLong Gold antifade reagent (Life Technologies Corporation, Eugene, OR, USA). The sections were examined by light microscope and lesions documented by fluorescence microscopy (VS120 Virtual Slide Microscope; Olympus) using the cellSense software for image capture and processing.

Data Analysis

The images of the retinal lesions obtained on D0 and D3 were analyzed by the first author for pathology in the neuroretina secondary to the photocoagulation, such as pale lesions on fundus photography or disruption of the normal retinal layering on OCT. At all follow-up examinations (D3–D42), signs of retinal fluid accumulation, tissue swelling, and subretinal density potentially representing a CNV were noted. The height of the subretinal densities were assessed as the distance from the level of the pigment epithelium to the top of the densities using the inbuilt marking tool of the OCT apparatus. The measurements were performed 3 times at random order with intervals of at least 2 weeks, which resulted in measurements of the heights of the densities with an average coefficient of variation (CV) of 1.53% for eyes without saline pretreatment and 1.30% for eyes pretreated with saline (overall CV 1.42%). For each lesion, the average of the three measurements was used as the measure of the height. The OCT angiograms were analyzed using the Imagenet software (Topcon) that automatically identifies four different layers in the retina (i.e. the superficial vascular plexus, the deep vascular plexus, and the outer retina and Bruch's membrane). In 10 cases, where the automatic identification of the retinal layers was aberrant, the positioning of the layer to be analyzed was corrected manually. It was noted whether the sites of the laser application showed perfused vessels in the outermost of the studied layers.

Fluorescein angiograms were evaluated by two independent graders, a retina specialist (author T.B.) and the first author (SH). The grader assessed whether fluorescence increased during the angiographic phases at the site of the laser application. Out of 57 examinations from 16 animals, the evaluation of 5 examinations were discrepant. In two of the cases, a grader had mistakenly evaluated an area not containing the laser application, and, in three cases, a unanimous conclusion was reached after the graders had studied the angiograms together.

Subsequently, a CNV was defined to be present if: (1) the site of the laser application presented with increased subretinal density on OCT scanning that (2) showed increasing hyperfluorescence during the angiographic phases by fluorescein angiography, or perfused vessels in the outer retinal layers by OCT angiography. At the 59 follow-up examinations, one OCT scan and 7 OCT angiograms were excluded due to insufficient image quality in the eyes treated with laser application only, and one OCT scan, 7 OCT angiograms, and 7 fluorescein angiograms were excluded in the pigs subjected to laser application after subretinal injection of saline.

Statistics

Graph Pad Prism version 8 was used for the statistical analyses. The Mann-Whitney test was used to test for significant changes in lesion height among the two groups at each time of examination. Additionally, for each group, the changes in lesion height over time was tested by mixed effect analysis.

Results

In all (16 of 16) eyes that received photocoagulation alone, the treatment resulted in whitish lesions in the fundus after 30 minutes. The lesions were accompanied by diffuse swelling of all neuroretinal layers as observed by OCT, whereas no changes were observed in the choroid (Fig. 2, upper panel).

In the eyes pretreated with subretinal saline, none of the eyes displayed visible pale lesions and OCT in all cases showed intact neuroretinal layers and no choroidal lesions were observable through the subretinal fluid after 30 minutes (Fig. 2, lower panel). In all eyes the subretinal fluid had resorbed and the site of photocoagulation had become visible on fundus photography on D3 (not shown). On D7, eyes treated with photocoagulation alone displayed white scars at the site of the laser application on fundus photographs, increased subretinal density and damage to the neuroretinal layers by OCT and a perfused CNV by angiography (Fig. 3, upper panel).

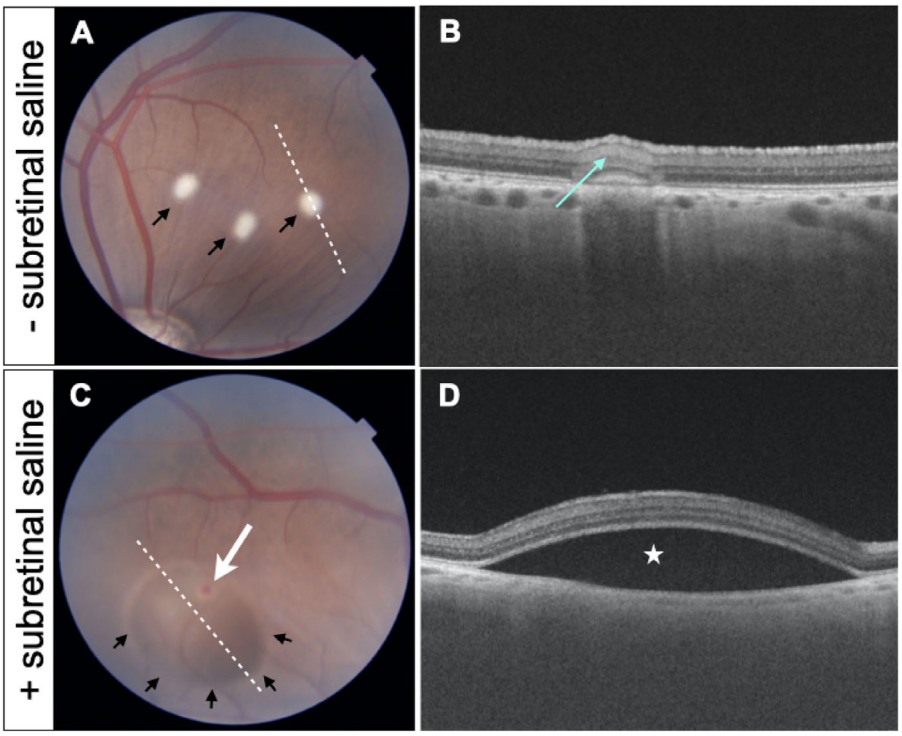

Figure 2. Representative examples of fundus photographs and OCT scans 30 minutes after photocoagulation alone (*upper panel*) and in the presence of subretinal saline (lower panel). (**A**) Fundus photograph with the three whitish photocoagulations (*arrows*). At the application a central bubble was observed in the right lesion, which was subsequently used as the study lesion. The dashed line represents the OCT scanning plane. (**B**) OCT scan of the rightmost lesion in **A**. The *arrow* points to the swellings of the neuroretina at the site of photocoagulation. (**C**) Fundus photograph of an eye pretreated with subretinal saline injection. The *black arrows* point to the margin of the serous detachment, but the photocoagulation burns cannot be observed. The *white arrow* points to the retinotomy. (**D**) OCT scan corresponding to the dashed line in **C**. The *asterisk* indicates the serous detachment underlying a retina without signs of thermic damage.

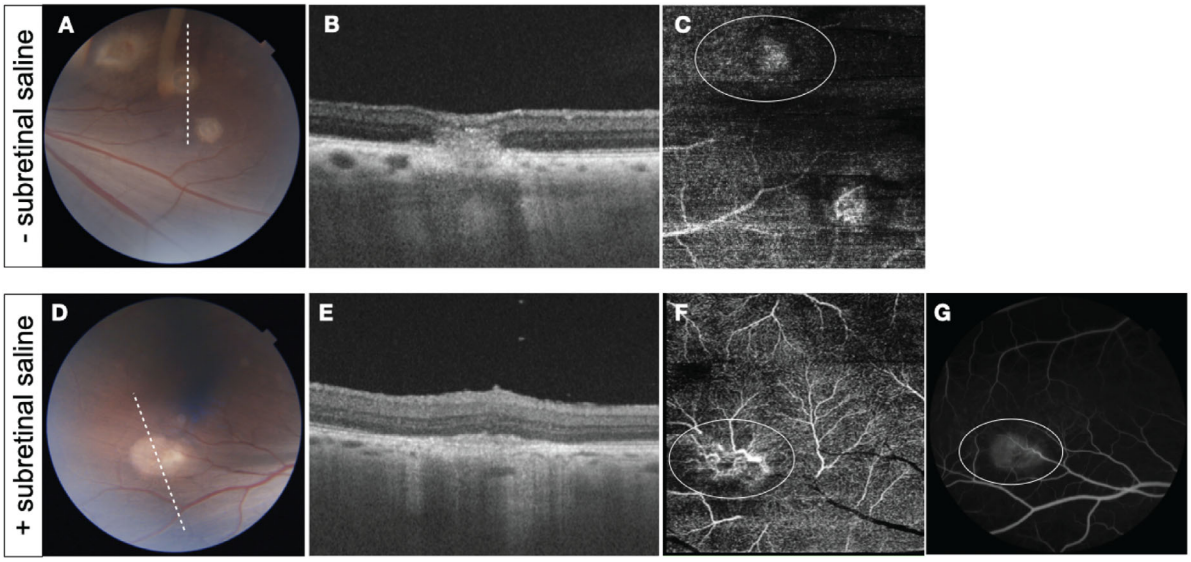

Figure 3. Examples of the development of a CNV as observed with the employed imaging techniques obtained on D7. *Upper panel*: After photocoagulation alone. (**A**) Fundus photograph with whitish scars. The *dashed line* corresponds to the scanning plane of the test lesion. (**B**) OCT scan corresponding to the dashed line in **A** showing increased subretinal density and damage to the inner retinal layers. (**C**) OCT angiogram showing perfused CNV surrounded by ellipse corresponding to the two rightmost lesions in **A**). *Lower panel* After pretreatment with subretinal saline. (**D**) Fundus photograph with a whitish scar. (**E**) OCT scan corresponding to the dashed line in **D** showing increased subretinal density but continuity of the layers in the neuroretina. (**F**) OCT angiogram showing perfused CNV surrounded by ellipse. (**G**) Fluorescein angiogram showing hyperfluorescence corresponding to the CNV.

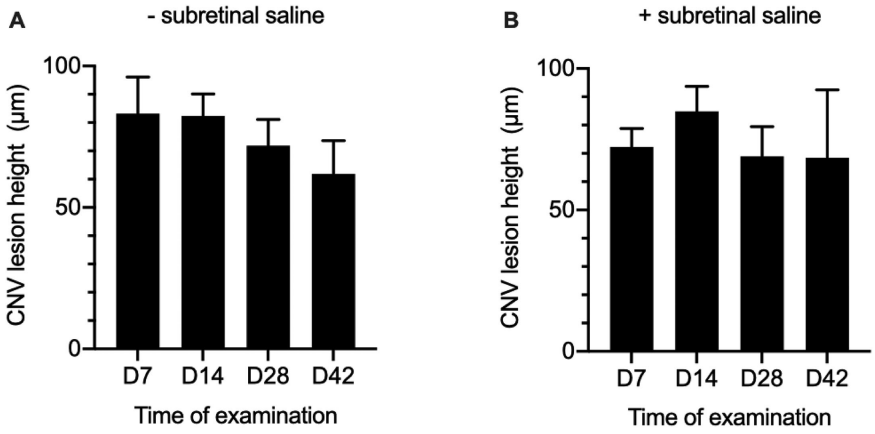

Figure 4. The height of the choroidal neovascularizations as a function of time of follow-up after photocoagulation. Error bars indicate standard error of the mean (SEM).

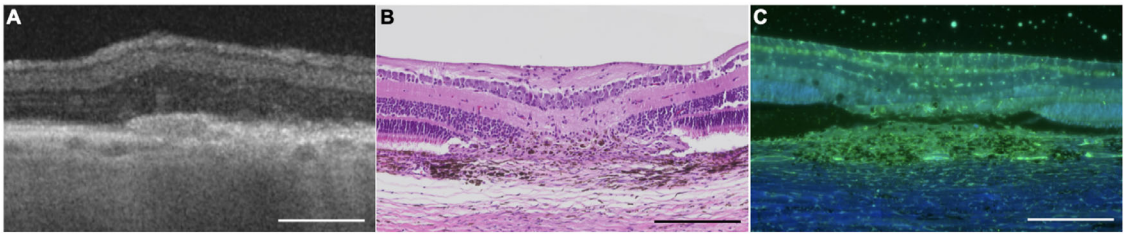

Figure 5. Representative example of a CNV membrane on D14 after photocoagulation in the presence of subretinal saline. Scale bar = 200 µm. (**A**) OCT scan through the lesion immediately before enucleation. (**B**) Hematoxylin and eosin staining of histological section showing fibrovascular material corresponding to the lesion. (**C**) The adjacent section stained cell nuclei with DAPI (*blue*) and endothelial cells with isolectin (*green*).

In eyes pretreated with subretinal saline, the appearance of CNVs on fundus photography, OCT angiography, and fluorescein angiography was similar to that of the eyes treated with photocoagulation alone. However, the subretinal densities observed by OCT were not accompanied with damage to the inner retinal layers. (Fig. 3, lower panel). On D7, where 14 pigs were still alive, CNVs could be identified in 11 of 14 of the eyes without pretreatment and in 11 of 14 of the eyes pretreated with subretinal saline injection. Increasing hyperfluorescence during the angiographic phases was observed in 10 of 14 eyes on D3, 8 of 13 eyes on D7, 5 of 12 eyes on D14, 5 of 12 eyes on D28, and in 1 of 5 eyes on D43. The reduction of the height of the subretinal lesions decreased over time, but the decrease was not significant, neither for the eyes treated with photocoagulation alone ($P = 0.35$) nor for the eyes pretreated with subretinal saline ($P = 0.28$, Fig. 4).

The histological examination at D14 after photocoagulation preceded by subretinal injection of saline showed lesions with hematoxylin and eosin staining of fibrovascular tissue invading the outer retina (Fig. 5).

Invasion of the outer retina by fibrovascular tissue was not observed in the animals euthanized at D0 to D3 but had started at D7 (data not shown).

Discussion

To our knowledge, this is the first study to show that experimental CNVs induced by retinal photocoagulation can be generated reproducibly without causing collateral damage to the neuroretina. Furthermore, the success rate for CNV induction was high, which may be a consequence of the careful titration of the laser power used to stimulate the neovascular response. This assured a localized and controlled penetration of Bruch's membrane, which has previously been shown to be essential for the induction of experimental CNV.[22] These preconditions may not

be present when the lesion to Bruch's membrane is performed by other types of traumatic intervention, such as surgical destruction.[16] In addition, the extension of thermic damage to the neuroretina induced coagulation necrosis in the inner retinal tissue.[16] This may eliminate retinal components that are involved in the development of CNV lesions in humans. These models can therefore be assumed to have limited value for drug development aimed at treating this condition.

Protection of the neuroretina from thermic damage was facilitated by subretinal injection of saline in which the forward expansion of heat from the photocoagulation could be absorbed. The fact that the subretinal fluid had resorbed at D3 allowed a comparable demonstration of the sites of the photocoagulation in the two groups at all follow-up examinations. It cannot be excluded that the laser application had affected neuroretinal function, but a possible impact could not be observed with the used imaging techniques. Additionally, the lack of intraretinal invasion of the CNV at D3 in the lesions protected by subretinal saline suggests that the neuroretina had not been primarily involved in the formation of the CNV. The histological examinations confirmed the OCT findings that invasion of CNVs into the neuroretina occurred from D7. Therefore, CNV induced in the presence of subretinal saline where the primary lesion is restricted to Bruch's membrane may better reflect the processes involved in CNV formation in nAMD. A disadvantage of photocoagulation in the presence of subretinal saline was that the effect could not be observed at the time of the application, which may have caused a larger variability of the lesions produced in these eyes. This precludes the adjustment of the effect to a level that is optimal for producing CNVs in animals with different pigmentation. Therefore, the technique requires titration of the laser effect before the photocoagulation intended to initiate a CNV is applied. In the present study, this titration was performed in the fellow eye of the animal, but in cases where the severity of the intervention, the study design, or animal ethical considerations should preclude intervention on both eyes, this titration would have to be done in the same eye with possible derived effects on the neovascular response. Real-time analysis of temperature distribution using recently developed methods,[18–20] may further optimize laser titration. It cannot be excluded that the effects of the application on the neuroretina in the eyes that were not pretreated with subretinal saline or the retinotomy produced in the eyes pretreated with subretinal saline could have affected the results. Possible advantages of pretreatment should also be weighed against the risks for hemorrhage that, in the present study, precluded the continuation of the experiment in two cases, and ultimately for the risk of retinal detachment.

Structural damage to Bruch's membrane is a common denominator for diseases characterized by CNV whether it be due to degenerative changes, such as in nAMD, pathological myopia, inflammation, connective tissue disorders, or traumas.[23–25] The experimental CNVs induced in the present study developed secondary to an acute thermal trauma, which differs substantially from the mechanisms involved in eliciting CNVs in retinal disease, such as nAMD. Furthermore, the translation of the present results to humans should consider that the age of the studied pigs was 3 to 4 months, which corresponds to the biological age of children[26] in whom the neovascular response is different from that of older persons.

However, in spite of these limitations, it is likely that the stimulation of growth in choroidal vessels induced by photocoagulation may have similarities with the processes that are active in retinal disease in humans and that the model can be used to test therapies aimed at inhibiting this neovascularization, such as gene therapy.[12] The use of OCT scanning, OCT angiography, and fluorescein angiography to monitor the interventions allowed the introduction of diagnostic procedures similar to those used in clinical studies. This also ensured that the same animals could be examined repeatedly and implied that only one animal had to be euthanized at each follow-up time. This reduced the number of animals needed to carry out the study with a consequent improvement of animal welfare.

The height of the CNV produced by focal photocoagulation appeared after 7 days and tended to gradually decrease from 14 days after the photocoagulation, which may reflect a normal healing response. This pattern of development was supported by the fluorescein angiographic findings of the highest proportion of lesions showing increasing hyperfluorescence during the angiographic phases during the first 2 weeks after photocoagulation. The finding confirms results from previous studies[27] and emphasizes that experimental CNVs differ from CNV lesions in nAMD and other retinal diseases where the stimulus that generates and maintains the neovascularization can be considered to be constant or to increase over time. This should be considered in the planning of, for example, gene therapy-based interventions aimed at reducing the development and growth of experimental CNV. The effect of such interventions should be quantifiable a few weeks after the induction of the experimental CNV, although this may limit the types of intervention that can be carried out and the translational value of the results.

Altogether, the study has shown that focal photocoagulation can induce experimental CNV in the porcine retina reproducibly, and that pretreatment with subretinal saline prevents primary neuroretinal damage similarly to what is observed in nAMD. Furthermore, the study has shown that the effect of interventions aimed at reducing the development of experimental CNV optimally should be evaluated within a few weeks after the photocoagulation used to stimulate CNV formation.

Acknowledgments

Supported by Aarhus University, Fight for Sight Denmark, Synoptikfonden, Maskinfabrikant Jochum Jensen og hustru Mette Marie Jensen's Foundation, and Købmand Marie Kirstine Jensen's Foundation.

Vitreo-retinal surgeon Jesper Eriksen is thanked for valuable advice on the surgical procedures and professor Jesper Hjortdahl for lending surgical equipment. The AU Health Bioimaging Core Facility is thanked for the use of equipment and technical assistance. The animal facility, Department of Clinical Medicine, Aarhus University, is thanked for housing the pigs and providing the operational setting.

Disclosure: **S. Hansen**, None; **A.L Askou**, None; **M. la Cour**, None; **T.J. Corydon**, None; **T. Bek**, None

References

1. Jin G, Ding X, Xiao W, et al. Prevalence of age-related macular degeneration in rural southern China: the Yangxi Eye Study. *Br J Ophthalmol*. 2018;102:625–630.
2. Keel S, Xie J, Foreman J, van Wijngaarden P, Taylor HR, Dirani M. Prevalence of age-related macular degeneration in Australia: the Australian National Eye Health Survey. *JAMA Ophthalmol*. 2017;135:1242–1249.
3. Wilde C, Poostchi A, Mehta RL, et al. Prevalence of age-related macular degeneration in an elderly UK Caucasian population - The Bridlington Eye Assessment Project: a cross-sectional study. *Eye (Lond)*. 2017;31:1042–1050.
4. Wong WL, Su X, Li X, et al. Global prevalence of age-related macular degeneration and disease burden projection for 2020 and 2040: a systematic review and meta-analysis. *Lancet Glob Health*. 2014;2:e106–e116.
5. Guimaraes TAC, Georgiou M, Bainbridge JWB, Michaelides M. Gene therapy for neovascular age-related macular degeneration: rationale, clinical trials and future directions. *Br J Ophthalmol*. 2021;105(2):151–157.
6. Ferris FL, 3rd, Wilkinson CP, Bird A, et al. Clinical classification of age-related macular degeneration. *Ophthalmology*. 2013;120:844–851.
7. Kliffen M, Sharma HS, Mooy CM, Kerkvliet S, de Jong PT. Increased expression of angiogenic growth factors in age-related maculopathy. *Br J Ophthalmol*. 1997;81:154–162.
8. Lai K, Landa G. Current choice of treatments for neovascular AMD. *Expert Rev Clin Pharmacol*. 2015;8:135–140.
9. Haller JA. Current anti-vascular endothelial growth factor dosing regimens: benefits and burden. *Ophthalmology*. 2013;120:S3–S7.
10. Askou AL, Pournaras JA, Pihlmann M, et al. Reduction of choroidal neovascularization in mice by adeno-associated virus-delivered anti-vascular endothelial growth factor short hairpin RNA. *J Gene Med*. 2012;14:632–641.
11. Askou AL, Benckendorff JNE, Holmgaard A, et al. Suppression of choroidal neovascularization in mice by subretinal delivery of multigenic lentiviral vectors encoding anti-angiogenic microRNAs. *Hum Gene Ther Methods*. 2017;28:222–233.
12. Askou AL, Alsing S, Benckendorff JNE, et al. Suppression of choroidal neovascularization by AAV-based dual-acting antiangiogenic gene therapy. *Mol Ther Nucleic Acids*. 2019;16:38–50.
13. Sanchez I, Martin R, Ussa F, Fernandez-Bueno I. The parameters of the porcine eyeball. *Graefes Arch Clin Exp Ophthalmol*. 2011;249:475–482.
14. Chandler MJ, Smith PJ, Samuelson DA, MacKay EO. Photoreceptor density of the domestic pig retina. *Vet Ophthalmol*. 1999;2:179–184.
15. Guduric-Fuchs J, Chen W, Price H, Archer DB, Cogliati T. RPE and neuronal differentiation of allotransplantated porcine ciliary epithelium-derived cells. *Mol Vis*. 2011;17:2580–2595.
16. Kiilgaard JF, Andersen MV, Wiencke AK, et al. A new animal model of choroidal neovascularization. *Acta Ophthalmol Scand*. 2005;83:697–704.
17. Lassota N, Kiilgaard JF, Prause JU, Qvortrup K, Scherfig E, la Cour M. Surgical induction of choroidal neovascularization in a porcine model. *Graefes Arch Clin Exp Ophthalmol*. 2007;245:1189–1198.
18. Brinkmann R, Koinzer S, Schlott K, et al. Real-time temperature determination during retinal photocoagulation on patients. *J Biomed Opt*. 2012;17:061219.

19. Müller HH, Ptaszynski L, Schlott K, et al. Imaging of temperature distribution and retinal tissue changes during photocoagulation by high speed OCT, *Proc. SPIE 7889, Optical Coherence Tomography and Coherence Domain Optical Methods in Biomedicine XV, 78890E* (February 15, 2011); Available at: https://doi.org/10.1117/12.874788.
20. Jain A, Blumenkranz M, Paulus Y, et al. Effect of pulse duration on size and character of the lesion in retinal photocoagulation. *Arch Ophthalmol*. 2008;126(1):78–85
21. Pennesi ME, Neuringer M, Courtney RJ. Animal models of age related macular degeneration. *Mol Aspects Med*. 2012;33:487–509.
22. Grossniklaus HE, Green WR. Choroidal neovascularization. *Am J Ophthalmol*. 2004;137:496–503.
23. Penfold P, Killingsworth M, Sarks S. An ultrastructural study of the role of leucocytes and fibroblasts in the breakdown of Bruch's membrane. *Aust J Ophthalmol*. 1984;12:23–31.
24. Spraul CW, Grossniklaus HE. Characteristics of Drusen and Bruch's membrane in postmortem eyes with age-related macular degeneration. *Arch Ophthalmol*. 1997;115:267–273.
25. Kilarski WW, Samolov B, Petersson L, Kvanta A, Gerwins P. Biomechanical regulation of blood vessel growth during tissue vascularization. *Nat Med*. 2009;15:657–664.
26. Tohyama S, Kobayashi E. Age-appropriateness of porcine models used for cell transplantation. *Cell Transplant*. 2019;28:224–228.
27. Lassota N, Kilgaard JF, la Cour, Scherfing E, Prause JU. Natural history of choroidal neovascularization after surgical induction in an animal model. *Acta Ophthalmol*. 2008;86:495–503.